ILASS Americas, 22nd Annual Conference on Liquid Atomization and Spray Systems, Cincinnati, OH, May 2010

Effect of Injection Pressures on GDI Spray and Atomization of Different Fuels

Ji Zhang, Shanshan Yao, Himesh Patel, and Tiegang Fang*
Department of Mechanical and Aerospace Engineering
North Carolina State University
Raleigh, NC 27695-7910 USA

Abstract

In this paper, the effect of injection pressure on the spray structure development and atomization for butanol, ethanol and isooctane was investigated. Two pressures of 7.0 MPa and 10.2 MPa were used for each fuel. Transient spray images were taken by using a high speed camera for visualization and cone angle analysis. SMD, DV(90) and particle size distribution were measured using a laser diffraction technique. The transient images clearly show the sac spray at the initial phase and the main spray structure at the developed phase. These two phases transition smoothly for both butanol and ethanol at both injection pressures, but are apparently separated for isooctane at 10.2 MPa. The main reason is attributed to the lower viscosity of isooctane. The cone angle at the developed phase for butanol and ethanol are consistently stable while isooctane presents large deviation. The largest cone angle value is observed for ethanol at both injection pressures, while butanol shows the smallest. Higher injection pressure leads to a smaller cone angle for each fuel, among which isooctane shows the largest decrease. The sac spray for all fuels produces large droplets, resulting in a large value of SMD and DV(90) at the initial phase. Particle size distribution shows similar profiles for each fuel at both injection pressures.

*Corresponding author: tfang2@ncsu.edu

Introduction

Liquid fuel atomization is critical to combustion and emissions in gasoline engines. Meanwhile, renewable alternative fuels, such as bio-butanol and bio-ethanol, have received much research attention due to the elevated fossil fuel depletion. Compared with conventional gasoline fuels, these bio-fuels have quite different chemical and physical properties, which can greatly affect the spray and combustion processes [1].

Blends of ethanol and gasoline are commonly used in specially modified gasoline engines, as illustrated by the large amount of ethanol production in Brazil since 1980s and in USA recently [2]. Moreover, ethanol is also known as a substitute to diesel to a certain blending ratio. Blends of ethanol in diesel have been widely researched in current compression ignition (CI) engines. It is suggested that engine performance including power, brake specific fuel consumption, brake thermal efficiency, etc., are not significantly reduced while the exhaust emissions (CO and NO_x) greatly decrease [3]. Ethanol-diesel blends up to 20% can be used very well in CI engine without any modification [4, 5]. However, since ethanol is fully miscible in water, its corrosion to the iron-contained parts in the fuel system dramatically reduces the lifetime of those parts as well as endangers seals [6]. This solvent characteristic of ethanol also prevents its transportation in current pipelines like pure gasoline, which is an important reason why only Brazil and USA produce ethanol as a vehicle fuel.

On the other hand, butanol presents similar attraction as ethanol in terms of emission control and renewable production, while its property is closer to gasoline compared to ethanol. The properties, including 87 octane number, reasonable energy density and low solubility in water, make it a potential substitute to ethanol and/or gasoline for engine application. It can be more easily applied to current gasoline transportation and storage system compared with ethanol, while it meets the demanding environmental regulation without sacrifice of engine performance. Among few researches into the potential application of butanol in engines, Thomas et al. [7] compared a direct-injection spark-ignition (DISI) engine performance using blends of ethanol (10% v/v gasoline) and butanol (10% v/v gasoline). The performance of butanol was similar to ethanol from an emission and combustion standpoint and decreases in fuel consumption. A kinetic modeling agreed well with a jet-stirred reactor and opposed diffusion flame experimental measurements [8]; however, few research has been concentrated on the fluid flow aspects of butanol application on direct injection injectors.

As a promising and fast developing technology, direct injection (DI) has become dominant in the new spark-ignition engines. It features higher thermal efficiency, higher power output, better transient response and more precise air-fuel ratio control [9]. An understanding of spray and fuel atomization is critical to optimizing the GDI injector in practical engines. Park et al. [10] revealed that pure bio-ethanol had larger particle size and smaller cone angle compared to bio-ethanol blended gasoline and pure gasoline, whereas they did not provide detailed particle size distribution.

In this paper, spray visualization and particle size measurements were conducted under different injection pressures to address the spray characteristics of pure butanol and ethanol for sprays used in direct injection gasoline engines. Spray structure and cone angle were analyzed, and the droplet size distribution and characterization parameters of atomization including DV(90) and Sauter mean diameter (SMD) were obtained. The effects of injection pressure and fuel property on the spray development and atomization were discussed.

Experiment Apparatus

Three fuels (butanol, ethanol, and isooctane) were used to study the effect of fuel properties on the spray structure and atomization. 2,2,4-Trimethylpentane was used to simulate gasoline for the sake of standard property compared to real gasoline. Table 1 lists the major characteristic properties of fuels.

The schematic of the experimental setup is illustrated in Figure 1. A Stanford pulse/delay generator (Model No. DG535) generates a pulse to trigger the driver of a Fuel Stratified Injection (FSI) injector, the high speed camera (Phantom® V4.3), or the Malvern® SprayTec particle size analyzer simultaneously. The spray was injected into the ambient air at 25 ^{o}C indoor environment. High speed spray images and particle size distribution were taken separately for each condition. Each condition was repeated five times for above mentioned measurements to ensure the repeatability. The injector used in this experiment is a commercial swirl type FSI injector from Bosch (Serial No. 0261500016). There is an angle between the injector centerline and the spray centerline as shown in the spray image (Figure 3). The injection pulse width was 2.4 ms in all experiments. The injection pressure was maintained constant by using a compressed nitrogen cylinder at different pressure levels which was controlled by a two stage pressure regulator. The injection pressures of 7.0 MPa and 10.2 MPa were used to test the three fuels.

The high speed camera was adjusted to run at a frame rate of 25,000 frames per second with an expose time of 7 μs and image resolution of 128×128, 8 bits per pixel. The corresponding physical resolution in images is approximately 0.167 mm/pixel. A Nikon 60mm micro lens was used. The spray was illuminated by a light source volumetrically. The camera was triggered by the TTL signal that was sent to injector driver. For a typical run, 64,255 frames were taken, of which the first 200 frames (8 ms) were stored to analyze the whole injection process.

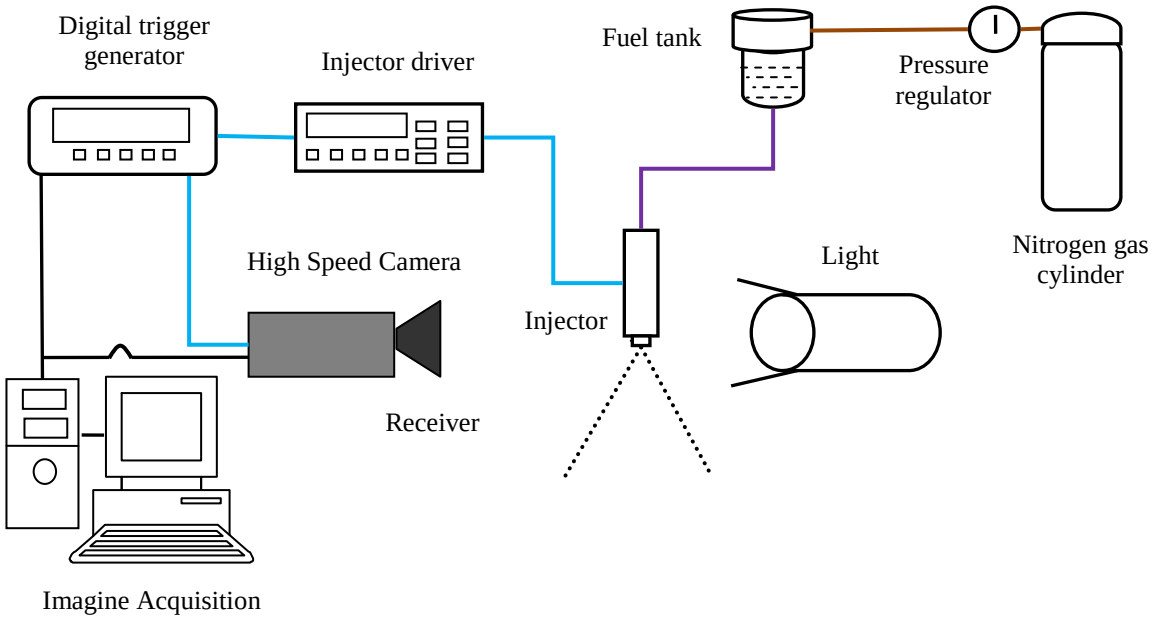

(a) Visualization system

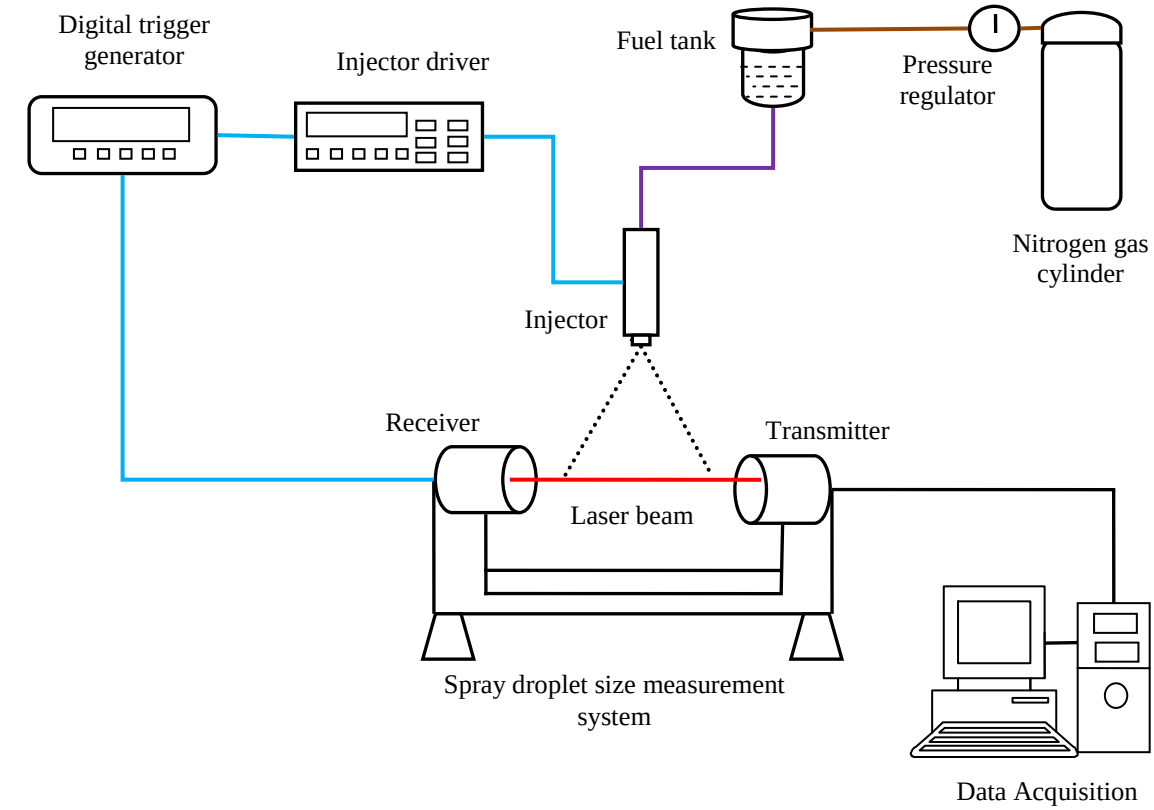

(b) Droplet size measurement system

Figure 1. Schematic of the experiment systems

Fuel	n-Butanol	Ethanol	Isooctane
IUPAC name	Butan-1-ol	Ethanol	2,2,4-Trimethylpentane
Structure formula	$CH_3(CH_2)_3OH$	CH_3CH_2OH	$(CH_3)_3CCH_2CH(CH_3)_2$
Density (kg/m^3 @ 20 °C)	809.8	789.67	688
Viscosity (mPa-s @ 20 °C)	3	2.41	1.04
Surface tension (N/m @ 20 °C)	0.025	0.023	0.022
MON	78	89	100
RON	96	107	100
LHV (MJ/kg)	33.075	26.9	44.3
Reid vapor pressure (kPa)	0.3	15.8	N/A
Stoichiometric air/fuel ratio	11.1	9	15.1
Flammability limits (%V Fuel in air)	1.4~11.3	3~19	1.4~7.6
Liquid heat capacity (kJ/kg.K @ 23 °C)	2.454	2.416	2.22
Solubility in water (ml/100 ml H_2O)	7.7	Fully miscible	<0.1

Table 1. Characteristic properties of fuels.

Spray images were processed by a Matlab® code to obtain the spray cone angle. The contrast of image was enhanced to facilitate edge detection. The threshold of 100 on [0, 255] grey scale was used for cone edge detection. This was selected to effectively detect the visible edge and exclude the recirculation zones at the spray edges. The detection area was restricted to the upstream of spray structure. The spray cone angle definition is illustrated in Figure 2. Starting from the appearance of stable spray to the detachment of spray from the nozzle, the images at every time step were processed to calculate the instantaneous cone angles. The cone angle in Figure 5 for each condition was the average of all the instantaneous values. Accordingly, the cone angle mainly represented the structure at the fully developed phase of a spray.

The particle size distribution of the spray was measured by a commercial SprayTec system that uses a laser diffraction technique. The Malvern® SprayTec was operated at a frequency of 10 kHz. A 300 mm lens was used in this measurement. The first 12 sets of optical detectors were disabled to eliminate beam steering effect, as instructed by the instrument manual. Vignetting effect was not observed in this measurement. The scattering threshold was 1. The measurement was triggered by the same TTL signal sent to the injector driver. A typical measurement spanned 20 ms after start of injection (ASOI). The nominal particle size was limited to between 0.1 µm and 500 µm. The laser beam passed through the centerline of the spray in the cross section which was 20 mm vertically from the injector tip (Figure 3). The evolution of the particle size distribution was obtained with respect to time for the analysis of the derived parameters.

For each condition, the time resolved particle size distribution was averaged on the basis of run numbers. Derived parameters and particle size distribution were obtained to quantitatively study the fuel atomization and development.

Figure 2. Cone angle definition

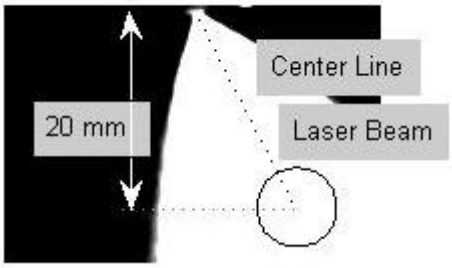

Figure 3. Laser beam position in laser diffraction experiments

Results and Discussion

Spray Structure and Cone Angle

The high speed spray images are shown in Figure 4 with injection pressures and time ASOI labeled. For each condition and fuel, two images were selected to present the initial and developed phases of spray development.

Butanol and ethanol show similar spray structure and development, both featuring faster spray penetration at the initial phase of 10.2 MPa injection pressure

compared to that at 7.0 MPa. At developed phase, spray appears smear and a relatively stable structure is observed. The transition from initial to developed phases is smooth.

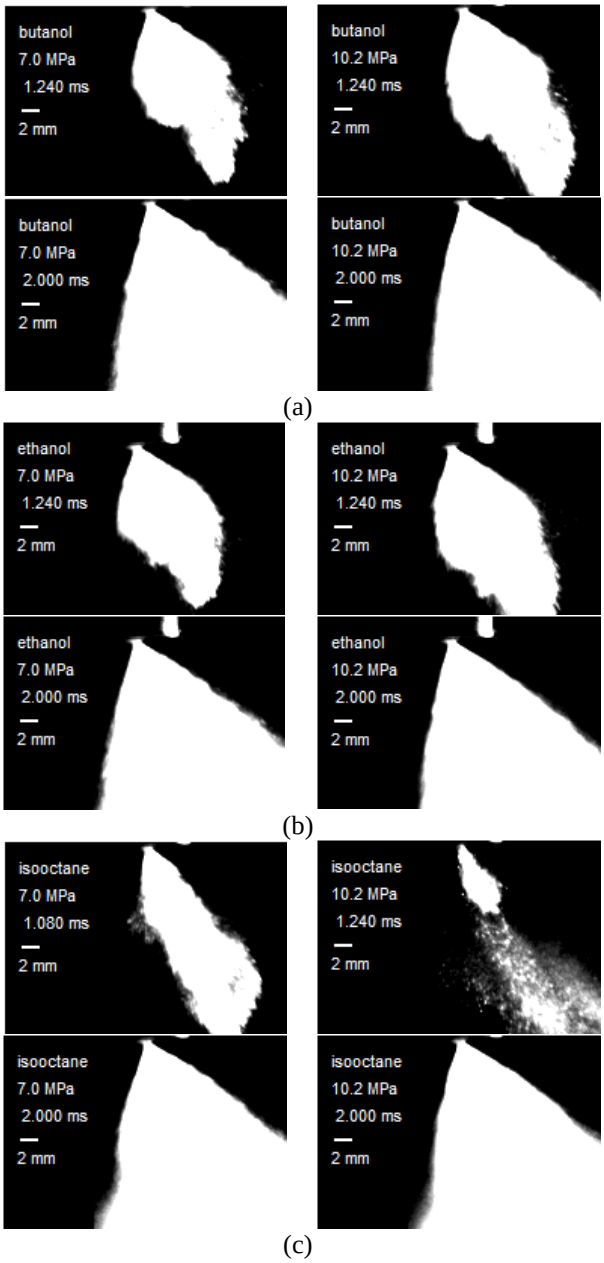

Figure 4. Spray structure images at 7.0 MPa and 10.2 MPa injection pressures and development phases: (a) butanol; (b) ethanol; (c) isooctane.

On the other hand, isooctane clearly shows existence of the two phases. To illustrate, a frame image with a slightly earlier time ASOI for isooctane at 7.0 MPa was selected. The sac spray at the initial phase is even separated from the main spray at the developed phase at 10.2 MPa, as depicted in Figure 4(c). The sac spray features a narrower cone and a faster penetration, because the sac volume of fuel is not accelerated in the swirl channels.

Due to a lower viscosity of isooctane compared to the other two oxygenated fuels, faster sac spray penetration was observed at both injection pressures. Even though the sac volume might be used to stabilize the stratified-charge combustion, due to its high momentum, it is generally expected that sac spray should be minimized because of the high risks to increase the overall mean droplet size, wall wetting and associated hydrocarbon emission [9].

Averaged cone angles for the three fuels at 7.0 MPa and 10.2 MPa are depicted in Figure 5. Ethanol shows the largest value at both injection pressures. A relatively large standard deviation is shown for isooctane at 7.0 MPa condition. As expected, higher injection pressure (10.2 MPa) reduces the cone angle value with approximately 1~3 degrees for the same fuel respectively, among which isooctane showed the largest decrease. Overall, the cone angle at the developed phase for different fuels does not change much with time.

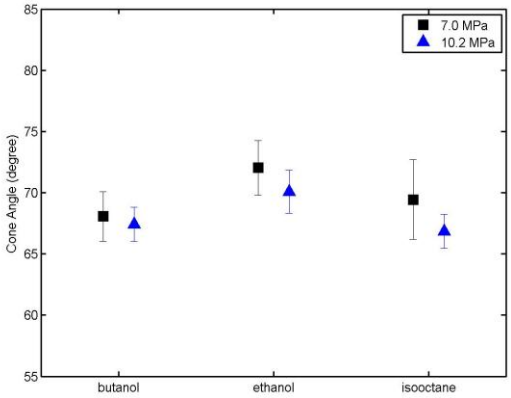

Figure 5. The averaged cone angle at developed phase for different fuels at 7.0 MPa and 10.2 MPa injection pressure. Error bar represents the standard deviation of obtained cone angels in the investigated time duration.

CHARACTERIZATION PARAMETERS FOR ATOMIZATION

To uncover more details of the spray evolvement, a spray event is divided into two phases, namely initial and developed phases, respectively. The initial phase (Phase 1) covers 0.5 ms time period after the particle data appears in the laser detectors. Phase 1 features the sac spray penetration, as discussed before. The developed phase (Phase 2) covers the event starting from 2.4 ms ASOI to the end of the injection event. Here 2.4 ms ASOI is selected in order to ensure that the start of Phase 2 includes the fully developed structure of the spray under different conditions; the end of the event represents the time after which no particles are de-

tected. Usually Phase 2 spans 2.5~2.8 ms depending on the injection pressures and fuels. There is a time gap of 0.1~0.3 ms between Phase 1 and 2 in certain cases, which is considered not to affect the result analysis since the characterization parameters are averaged values over the defined time range.

As shown in Table 2, for each fuel and injection pressure, Phase 1 features larger particles compared to Phase 2. This is also confirmed from the high speed images of sprays. More specifically, at the low injection pressure, butanol shows the largest SMD at Phase 1 and the smallest SMD at Phase 2; ethanol and isooctane shows similar SMD at Phase 1 but ethanol has a smaller SMD than isooctane at Phase 2.

Interestingly, the high injection pressure does not reduce SMD at Phase 2 for butanol and ethanol compared to isooctane, although SMD decreases at Phase 1 for these two fuels at a higher injection pressure. At the high injection pressure, three fuels present similar performance at Phase 1, implying a potential limit of atomization of fuels at this phase. Indeed, evidenced from the images, larger particles and poor atomization were visible at the initial phase. It will be doubtful that the atomization could be improved only by further increasing the injection pressure during Phase 1. On the contrary, butanol and ethanol show similar small particle sizes opposed to that of isooctane during Phase 2, indicating a good performance of these two fuels at the developed phase.

Injection Pressure (MPa)		DV(90) (μm)		D[3,2] (μm)	
	Phase	1	2	1	2
Butanol	7.0	112.3	45.6	31.6	10.3
	10.2	85.0	37.8	23.4	14.8
Ethanol	7.0	96.1	38.3	27.6	11.1
	10.2	91.7	34.2	23.3	14.9
Isooctane	7.0	110.3	55.1	28.6	17.1
	10.2	124.3	54.9	27.0	15.7

Table 2. Characterization parameters for different fuels at 7.0 MPa and 10.2 MPa injection pressure. Phases 1 and 2 represent initial and developed phases of spray evolvement.

In terms of injector design, the SMD at Phase 2 at both 7.0 and 10.2 MPa for different fuels shows a well addressed design for the main spray. DV(90) at Phase 2 is expected to decrease in an evaporating environment like engine cylinder. However, the large values of SMD and DV(90) for all fuels at Phase 1 indicate that further improvement to control sac spray is needed. Although the specific redesign of injector needs consideration of combustion requirement and/or mechanical restriction, the possible improvements may include, but not limited to, optimization of the swirl channels, reconfiguration of nozzle hole and sac chamber, modification of nozzle exit shape, etc.

PARTICLE SIZE DISTRIBUTION

Particle size distribution (PSD) profiles for different fuels at 7.0 MPa and 10.2 MPa are shown in Figure 6. Isooctane presents a certain portion of comparably larger particles (~100 μm) at both low and high injection pressures, which resulted in a higher SMD.

PSD profiles for different fuels are comparable at 7.0 MPa injection pressure, as opposed to that at 10.2 MPa injection pressure. At the high pressure, although the particle size of the largest component in PSD of isooctane is smaller than that of butanol and ethanol, the relatively large portion of large particles has made isooctane present a larger SMD and DV(90). Butanol and ethanol show similar PSD at both injection pressures.

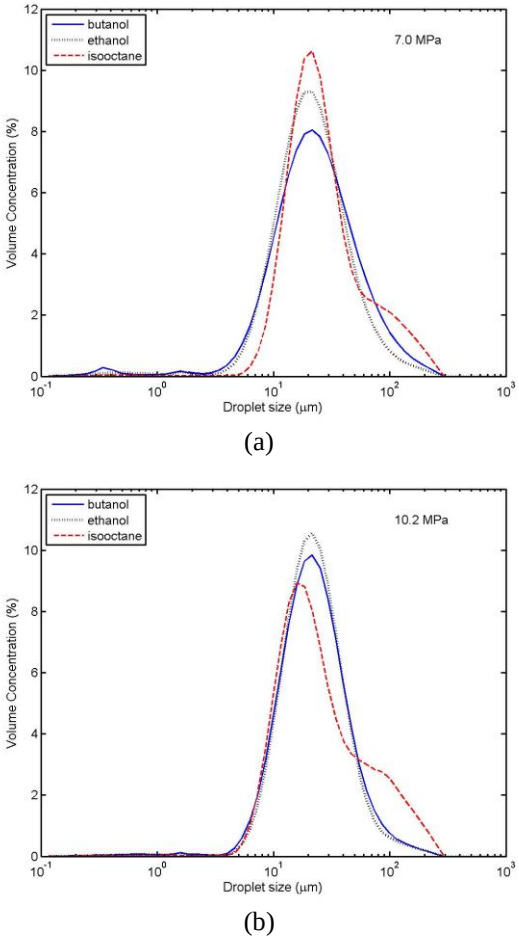

Figure 6. Particle size distribution (PSD) for different fuels at 7.0 MPa (a) and 10.2 MPa (b) injection pressure. Averaged over run times and time span when particle is detectable.

Conclusion

A series of experiments was conducted to investigate the effect of the injection pressure on the spray structure development and atomization characteristics for butanol, ethanol and isooctane. Transient spray images were taken via a high speed camera for visualization and cone angle analysis. SMD, DV(90) and particle size distribution were measured using a laser diffraction technique.

Spray structure develops smoothly for butanol and ethanol at both injection pressures of 7.0 and 10.2 MPa, while for isooctane, the initial spray and fully developed spray are apparently separated. The lower viscosity of isooctane may account for this difference compared to butanol and ethanol. The sac spray for all fuels produces large droplets, resulting in a large value of SMD and DV(90) at the initial phase. Particle size distribution shows similar profile for each fuel at both injection pressures.

Ethanol shows the largest cone angle value in all cases while isooctane shows the largest deviation at the low injection pressure. Butanol and ethanol perform consistently and similarly at both injection pressures. A higher injection pressure generates smaller cone angles for each fuel, among which isooctane shows the largest decrease.

References

1. Agarwal, A. K., *Progress in Energy and Combustion Science,* 33: p. 233-271 (2007).
2. Berg, C. and Licht, F. O., *World fuel ethanol, analysis and outlook*. 2004.
3. Al-Farayedhi, A. A., Al-Dawood, A. M., and Gandhidasan, P., *Journal of Engineering for Gas Turbines and Power,* 126: p. 178-191 (2004).
4. Meiring, P., Hansen, A. C., Vosloo, A. P., and Lyne, P. W. L. *SAE Technical Paper 831360*, 1983, pp.
5. Mouloungui, Z., Vaitilingom, G., Berge, J. C., and Caro, P. S., *Fuel,* 80: p. 565-74 (2001).
6. Hardenberg, H. O. and Ehnert, E. R. *SAE Technical Paper 811212*, 1981, pp.
7. Thomas, W., Scott, A. M., and Steve, M., *Journal of Engineering for Gas Turbines and Power,* 131: p. 032802 (2009).
8. Sarathy, S. M., Thomson, M. J., Togb, C., Dagaut, P., Halter, F., and Mounaim-Rousselle, C., *Combustion and Flame,* 156: p. 852-864 (2009).
9. Zhao, F., Lai, M. C., and Harrington, D. L., *Progress in Energy and Combustion Science,* 25: p. 437-562 (1999).
10. Park, S. H., Kim, H. J., Suh, H. K., and Lee, C. S., *International Journal of Heat and Fluid Flow,* 30: p. 1183-1192 (2009).